Modelling Pulsatile Blood Flow Using Casson Fluid Model Through an Overlapping Stenotic Artery with Au-Cu Hybrid Nanoparticles: Varying Viscosity Approach

Rishu Gandhi(✉) and B. K. Sharma

Department of Mathematics, Birla Institute of Technology and Science, Pilani, Pilani, Rajasthan, India
I.rishugandhi155@gmail.com

Abstract. The present study aims to perform computer simulations of two-dimensional hemodynamics of blood flow through an overlapping stenosed artery considering the non-Newtonian Casson fluid model to simulate the arterial region's hemorheological properties and hematocrit-dependent viscosity to mimic the realistic behavior of blood with a uniform magnetic field applied in the radial direction of the blood flow, motivated by magneto-hemodynamics effects. This study is influenced by drug delivery applications and proposes a mathematical model for unsteady blood flow using hybrid biocompatible nanoparticles (Gold and Copper). The Crank-Nicolson method solves the transformed governing equations with accompanying boundary conditions. For a given critical height of the stenosis, key hemodynamic variables such as velocity, wall shear stress, temperature, and flow rate are computed. The velocity and temperature profiles show enhancement as the Casson fluid parameter (β) increases. The velocity, wall shear stress, and flow rate of the fluid (blood) decline with an increment in the hematocrit parameter (h_m). A comparative study with published work is done to validate the current model, which is in good accord with the previous work. The findings may act as a benchmark for formulating the best regimens for the targeted treatment of atherosclerosis, obstructed hemodynamics, nano-hemodynamics, nano-pharmacology, blood purification systems, and treatment of hemodynamic ailments.

Keywords: Hematocrit-dependent viscosity · Overlapping stenosis · Au-Cu/Blood hybrid nanofluid · Pulsatile blood flow

1 Introduction

Nanofluids have gained popularity as a significant development in biomedical engineering in recent years. Theoretical and practical studies on the possible applications of nanoparticles in blood flow issues have significantly influenced

J. Singh et al. (Eds.): ICMMAAC 2022, LNNS 666, pp. 155–176, 2023.
https://doi.org/10.1007/978-3-031-29959-9_10

Nomenclature

r_1^*	Radial direction	d	location of stenosis
z_1^*	Axial direction	L_0	length of stenosis
t_1^*	Time	M^2	Magnetic Number
u_1^*	Velocity component in radial direction	Re	Reynold's Number
w_1^*	Velocity component in axial direction	Gr	Grashof Number
U_0	Reference velocity	Pr	Prandtl Number
R	Radius of artery in stenotic region	Q_1	Flow Rate
R_0	Radius of artery in non-stenotic region	***Greek Letters***	
g	Acceleration by virtue of gravity	δ	Stenosis depth
$h(r_1^*)$	volume fraction of RBCs	β	Casson Fluid Parameter
h_m	maximum hematocrit at artery's center	σ	Electrical conductivity
$\tilde{T}^*$	Temperature of the base fluid	$\tilde{\theta}$	Non-dimensional temperature
$\tilde{T}_1^*$	Reference temperature	ρ	Density
$\tilde{T}_w^*$	Temperature at the wall	ϕ_1	Volume fraction of Au-NPs
B_0	Uniform Magnetic Field	ϕ_2	Volume fraction of Cu-NPs
$\tilde{C}_p^*$	Specific heat at constant pressure	γ	Thermal expansion coefficient
k_f	Thermal conductivity	τ_w	Shear stress at the wall
p_1^*	Pressure	μ_0	coefficient of viscosity of plasma
w_s	Wall slip velocity	μ_f	Blood's viscosity

current bio-science literature. Many nanoparticle applications include gene therapy, MRI, tracking agents, and surgical tools for treating hyperthermia. Gold nanoparticles transport and unload drugs using their unique physical and chemical properties. Ghosh et al. [1] investigated the role of gold nanoparticles in drug administration. Gentile et al. [2] investigated the effects of vascular permeability on blood transport with nanoparticle suspension via blood vessels. The impact of the slip condition on blood flow through a tapering stenosed artery in the presence of nanoparticles was examined by Nadeem and Ijaz [3]. Using nanoparticles, Bahrami et al. [4] studied cancer therapy through targeted drug delivery. They found that nanoparticles have proven to be a successful technique that can lessen the side effects of current anti-cancer drugs. Gupta et al. [5] examined the MHD 2D-flow of Williamson-type nanofluid using nonlinear thermal radiation, Cattaneo-Christov heat and mass flux models. Under the influence of the magnetic field, Umadevi et al. [6] examined the blood flow suspended with Cu-nanoparticles via an inclined artery having overlapping stenosis. Gandhi et al. [7] constructed a mathematical model for drug delivery using Au-Al_2O_3/Blood hybrid nanoparticles via a bell-shaped stenosed artery. Gandhi and Sharma [8] studied the influence of hybrid nanoparticles on two-dimensional pulsatile blood flow through a vertical artery with irregular stenosis with an inclined external magnetic field. Using Au and GO nanoparticles, Khanduri and Sharma [9] investigated the influence of Hall and ion slips on MHD blood flow through a catheterized multi-stenosis artery with thrombosis.

A frequent cause of cardiovascular disease in coronary arteries is the buildup of fatty substances inside the artery wall lumen. This mechanism limits the amount of oxygenated blood that may leave the heart and travel to the rest of the body by decreasing the radius of blood arteries while raising blood flow resistance. The hemodynamical study in stenosed arteries is a crucial field of research because of its vital applications in cardiovascular illnesses like angina, heart attacks, atherosclerosis, and aneurysms, which are among the world's top causes of death. Numerous theoretical and practical research efforts have been conducted to gain a deeper understanding of the factors contributing to stenosis formation and its effects on blood flow dynamics. Several researchers [10–13] have mathematically explored the blood flow via arteries with overlapping stenosis. Sharma et al. [14] utilized blood as biomagnetic fluid to explore Soret and Dufour's effects via a stenosed artery having tapering effects. Under the impact of a uniform magnetic field, Das et al. [15] investigated the physical repercussions of suspension of hybrid nanoparticles in blood moving via porous artery with inclination having minor stenosis. Using a two-phase mixing approach, Zhang et al. [16] studied the impacts of nanoparticle volume fraction on plaque disintegration during transit. Basha et al. [17] investigated the fluid transport behavior of Au-Cu/Blood hybrid nanofluid via an artery having the inclination and irregular stenosis. Gandhi et al. [18] performed entropy generation analysis for blood flow through an irregular stenosed artery utilizing hybrid nanoparticles of different shapes. Using hematocrit-dependent viscosity, Sharma et al. [19] examined the effects of heat transfer and body acceleration on unsteady MHD blood flow in a curved artery in the presence of stenosis and aneurysm.

Most of the research described above examined the connection between artery stenosis and blood flow dynamics while treating blood as a Newtonian fluid. The blood behaves in the larger-diameter arteries with an assertive Newtonian behavior when shear rates are greater than 100 s^{-1}. However, because blood is a suspension of cells, it is widely known that arteries with smaller diameters and lower shear rates exhibit greater non-Newtonian blood behavior. The Casson fluid flow model has acquired popularity recently due to its fascinating application in human life. In today's science, the Casson fluid flow model has significant demand. Casson fluid demonstrates yield stress features. When the yield stress is high enough, the Casson fluid transforms into the Newtonian fluid. Sarifuddin et al. [20] explored the effect of two-dimensional blood flow, considering blood to be Casson fluid via an irregular stenosed artery employing the Marker and Cell approach for solving the equations numerically. Debnath et al. [21] studied the influence of a 1^{st}-order homogeneous-heterogeneous chemical reaction in an annular pipe, using the Casson model to characterize the liquid's non-Newtonian viscosity. Ali et al. [22] used Darcy's law to investigate the flow behavior of Casson fluid via a 2-D porous channel employing a vorticity-stream function approach. Tassaddiq et al. [23] examined the Newtonian heating effects for the generalized Casson fluid flow utilizing a Mittag-Leffler fractional operator. Using the Elzaki transform method and Elzaki decomposition approach, Sushila et al. [24] studied the thin film flow of a third-grade fluid down an inclined plane. Das et al. [25] investigated solute dispersion through a stenotic tube with

an absorptive wall, and Casson fluid describes the rheology of blood. Padma et al. [26] aimed to investigate how yield stress affected the EMHD motion of Casson fluid and nanoparticles as they flow via a mildly blocked inclined tapering artery.

The present research is inspired by the potential for nanoparticles to serve as efficient drug delivery and transport systems, given their capacity to hold significant quantities of therapeutic substances. Since blood is considered a non-Newtonian fluid, small-sized nanoparticles are becoming increasingly common in biomedical applications. Therefore, nanoparticles can either stimulate or inhibit blood vessel formation. Although some medications can increase or decrease blood-capillary expansion in some conditions, they only work for a short duration. Recently, researchers found that using these nanoparticles might resolve previously identified medication administration problems. Based on the literature survey performed above, no effort has been yet made to study the two-dimensional pulsatile hybrid nanofluid flow through an overlapping stenosed artery incorporating gold and copper nanoparticles considering blood as non-Newtonian Casson fluid with variable viscosity dependent on hematocrit under the influence of radiation and magnetic field effects. The present study seeks to perform computer simulations of two-dimensional hemodynamics of blood flow through an overlapping stenosed artery using the non-Newtonian Casson fluid model to simulate the arterial region's hemorheological properties and hematocrit-dependent viscosity to mimic the realistic behavior of blood with a uniform magnetic field applied in the radial direction of the blood flow. The pulsatile pressure gradient effects portray actual blood flow in unsteady flow situations. The novelty of the mathematical model formulated in the present analysis is as follows:

- To evaluate the impact of hybrid nanoparticles (Au + Cu) through an overlapping stenotic artery influenced by an external magnetic field and radiation, considering wall slip effects.
- Utilizing the Casson fluid model to address the non-Newtonian features of blood along with the hematocrit-dependent viscosity model to analyze the variable viscosity.

2 Mathematical Formulation

An unsteady, laminar, incompressible, viscous electrically conducting MHD blood flow through an inclined artery with overlapping stenosis is considered. A cylindrical coordinate system (r_1^*, $\tilde{\theta}$, z_1^*) is employed with r_1^* and z_1^* as radial and axial directions respectively. The axial symmetry of the artery corresponds to the independence of flow in the azimuthal ($\tilde{\theta}$) direction. The blood behavior is assumed non-Newtonian and is represented using Casson fluid model. The variable viscosity which is dependent on hematocrit is employed. A uniform magnetic field B_0 is applied to the blood flow in the radial direction. The magnetic Reynold's number is assumed very small ($\mathrm{Re} \ll 1$); therefore, the induced magnetic field is neglected compared to the applied magnetic field.

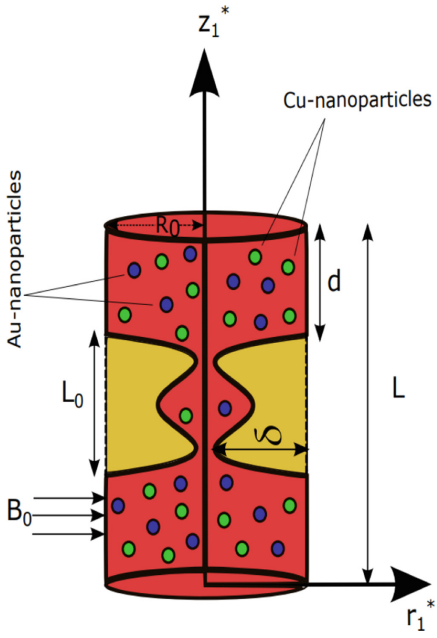

Fig. 1. The overlapping stenotic artery doped with hybrid nanoparticles

The geometry of the overlapping stenosis is assumed as [13]:

$$R(z_1^*) = \begin{cases} R_0\left[1 - \frac{64}{10}\eta_1\left(\frac{11}{32}L_0^3(z_1^* - d) + \frac{47}{48}L_0^2(z_1^* - d)^2 - L_0(z_1^* - d)^3 \right.\right. \\ \qquad \left.\left. + \frac{1}{3}(z_1^* - d)^4\right)\right], \qquad d \le z_1^* \le d + 3L_0/2, \\ R_0, \qquad \text{otherwise.} \end{cases} \tag{1}$$

The parameter η_1 is defined as:

$$\eta_1 = \frac{4\delta}{R_0 L_0^4}$$

where δ is the critical height of the stenosis occuring at two different positions, i.e.,

$$z_1^* = d + \frac{8L_0}{25}, \quad \text{and} \quad z_1^* = d + \frac{61L_0}{50}$$

The blood viscosity is affected by several parameters, including plasma viscosity, protein level, red blood cell concentration, strain rate and temperature. The concentration of red blood cells or hematocrit is one of these factors that significantly impact blood viscosity. Blood viscosity at a distance of r_1^* from an artery's axis can be described as

$$\mu_f = \mu_0[1 + \beta_1 h(r_1^*)], \tag{2}$$

and the expression for the hematocrit, $h(r_1^*)$ is given as -

$$h(r_1^*) = h_m \left[1 - \left(\frac{r_1^*}{R_0}\right)^m\right] \tag{3}$$

where β_1 has value 2.5 for blood and m is the control parameter for the shape of the blood velocity profile ($m \geq 2$).

2.1 Governing Equations

The blood flow through an inclined overlapping stenosed artery (Fig. 1) is assumed to be bidirectional. Therefore, the velocity and temperature fields are represented as:

$$\tilde{V}^* = \tilde{V}^*[u_1^*(r_1^*, z_1^*, t_1^*),\ 0,\ w_1^*(r_1^*, z_1^*, t_1^*)]\ , \qquad \tilde{T}^* = \tilde{T}^*(r_1^*, z_1^*, t_1^*)$$

The Casson fluid model's rheological equation of state for an incompressible flow is as follows:

$$\tau_{ij}^* = \begin{cases} 2\left(\mu_b^* + \frac{p_y^*}{\sqrt{2\pi^*}}\right)e_{ij}^*, & \pi^* > \pi_c^* \\ 2\left(\mu_b^* + \frac{p_y^*}{\sqrt{2\pi_c^*}}\right)e_{ij}^*, & \pi^* \leq \pi_c^* \end{cases} \tag{4}$$

where $\pi^* = e_{ij}^*.e_{ij}^*$ is the product of deformation rate with itself, π_c^* is a critical value based on the non-Newtonian model, μ_b^* is the plastic dynamic viscosity of the non-Newtonian fluid, and p_y^* is the yield stress of the fluid.

When $\pi^* \leq \pi_c^*$, Eq. (4) can be expressed as:

$$\tau_{ij}^* = 2\mu_b^*\left(1 + \frac{1}{\beta}\right)e_{ij}^* \tag{5}$$

where $\beta = \frac{\mu_b^*\sqrt{2\pi_c^*}}{p_y^*}$ is the Casson fluid parameter.

Under the above assumptions and invoking the Boussinesq approximation, the continuity equation, momentum equation and energy equation are represented as:

Continuity Equation:

$$\frac{\partial u_1^*}{\partial r_1^*} + \frac{u_1^*}{r_1^*} + \frac{\partial w_1^*}{\partial z_1^*} = 0, \tag{6}$$

Momentum Equation:

r-direction:

$$\rho_{hnf}\left[\frac{\partial u_1^*}{\partial t_1^*} + u_1^*\frac{\partial u_1^*}{\partial r_1^*} + w_1^*\frac{\partial u_1^*}{\partial z_1^*}\right] = -\frac{\partial p_1^*}{\partial r_1^*} + \frac{1}{r_1^*}\frac{\partial}{\partial r_1^*}\left[\mu_{hnf}\left(1+\frac{1}{\beta}\right)r_1^*\frac{\partial u_1^*}{\partial r_1^*}\right]$$
$$+ \frac{1}{2}\frac{\partial}{\partial z_1^*}\left[\mu_{hnf}\left(1+\frac{1}{\beta}\right)\left(\frac{\partial w_1^*}{\partial r_1^*} + \frac{\partial u_1^*}{\partial z_1^*}\right)\right] - \mu_{hnf}\left(1+\frac{1}{\beta}\right)\frac{u_1^*}{r_1^{*2}}, \tag{7}$$

z-direction:

$$\rho_{hnf}\left[\frac{\partial w_1^*}{\partial t_1^*} + u_1^*\frac{\partial w_1^*}{\partial r_1^*} + w_1^*\frac{\partial w_1^*}{\partial z_1^*}\right] = -\frac{\partial p_1^*}{\partial z_1^*} + \frac{1}{2}\frac{1}{r_1^*}\frac{\partial}{\partial r_1^*}\left[\mu_{hnf}\left(1+\frac{1}{\beta}\right)r_1^*\left(\frac{\partial u_1^*}{\partial z_1^*} + \frac{\partial w_1^*}{\partial r_1^*}\right)\right]$$
$$+ \frac{\partial}{\partial z_1^*}\left[\mu_{hnf}\left(1+\frac{1}{\beta}\right)\frac{\partial w_1^*}{\partial z_1^*}\right] + (\rho\gamma)_{hnf}g(\tilde{T}^* - \tilde{T}_1^*) - \sigma_{hnf}B_0^2 w_1^*, \tag{8}$$

Energy Equation:

$$(\rho C_p)_{hnf}\left[\frac{\partial \tilde{T}^*}{\partial t_1^*} + u_1^*\frac{\partial \tilde{T}^*}{\partial r_1^*} + w_1^*\frac{\partial \tilde{T}^*}{\partial z_1^*}\right] = k_{hnf}\left[\frac{\partial^2 \tilde{T}^*}{\partial r_1^{*2}} + \frac{1}{r_1^*}\frac{\partial \tilde{T}^*}{\partial r_1^*} + \frac{\partial^2 \tilde{T}^*}{\partial z_1^{*2}}\right] - \frac{\partial q_r^*}{\partial r_1^*}, \tag{9}$$

where

$$q_r^* = -\frac{4\sigma_e}{3k_e}\frac{\partial T^4}{\partial r_1^*}, \tag{10}$$

It is assumed that there are minimal temperature changes within the blood flow. Therefore, $\tilde{T}^4$ in Eq. (10) is linearized by disregarding higher-order terms and is expanded using Taylor series around $\tilde{T}_1^*$:

$$\tilde{T}^{*4} = 4\tilde{T}_1^{*3}\tilde{T} - 3\tilde{T}_1^{*4},$$

Hence, Eq. (10) becomes

$$q_r^* = -\frac{16\tilde{T}_1^{*3}\sigma_e}{3k_e k_f}\frac{\partial \tilde{T}}{\partial r_1^*}.$$

The boundary conditions are:

$$\frac{\partial w_1^*}{\partial r_1^*} = 0, \frac{\partial \tilde{T}^*}{\partial r_1^*} = 0 \quad \text{at} \quad r_1^* = 0, \tag{11}$$

$$w_1^* = w_s, \tilde{T}^* = \tilde{T}_w^* \quad \text{at} \quad r_1^* = -R, R, \tag{12}$$

The initial assumptions regarding velocity and temperature are considered as:

$$w_1^* = 0, \tilde{T}^* = 0 \quad \text{at} \quad t_1^* = 0. \tag{13}$$

Table 1. Thermophysical parameters of nanofluid and hybrid nanofluid [18,27]

Properties	Mathematical expression for nanofluid and hybrid nanofluid
Viscosity	$\mu_{hnf} = \frac{\mu_{nf}}{(1-\phi_1)^{2.5}(1-\phi_2)^{2.5}}$
Density	$\rho_{hnf} = [(1-\phi_2)\{(1-\phi_1)\rho_f + \phi_1\rho_{s_1}\}] + \phi_2\rho_{s_2}$
Heat Capacity	$(\rho C_p)_{hnf} = [(1-\phi_2)\{(1-\phi_1)(\rho C_p)_f + \phi_1(\rho C_p)_{s_1}\}]$
Thermal Conductivity	$\frac{k_{hnf}}{k_{bf}} = \frac{k_{s_2}+(m-1)k_f-(m-1)\phi_2(k_f-k_{s_2})}{k_{s_2}+(m-1)k_f+\phi_2(k_f-k_{s_2})}$
	where $\frac{k_{bf}}{k_f} = \frac{k_{s_1}+(m-1)k_f-(m-1)\phi_1(k_f-k_{s_1})}{k_{s_1}+(m-1)k_f+\phi_1(k_f-k_{s_1})}$
Electrical Conductivity	$\frac{\sigma_{hnf}}{\sigma_{bf}} = \frac{\sigma_{s_2}+(m-1)\sigma_f-(m-1)\phi_2(\sigma_f-\sigma_{s_2})}{\sigma_{s_2}+(m-1)\sigma_f+\phi_2(\sigma_f-\sigma_{s_2})}$
	where $\frac{\sigma_{bf}}{\sigma_f} = \frac{\sigma_{s_1}+(m-1)\sigma_f-(m-1)\phi_1(\sigma_f-\sigma_{s_1})}{\sigma_{s_1}+(m-1)\sigma_f+\phi_1(\sigma_f-\sigma_{s_1})}$
Thermal Expansion Coefficient	$\gamma_{hnf} = [(1-\phi_2)\{(1-\phi_1)\gamma_f + \phi_1\gamma_{s_1}\}] + \phi_2\gamma_{s_2}$

Table 2. Default Values of emerging parameters

Parameters	ϕ_1	ϕ_2	d	B_1	c_1	e	δ	β	w_s	β_1	h_m
Value	0.03	0.03	1	1.41	1	0.2	0.1	2	0.1	2.5	0.5

Table 3. Thermophysical properties of nanoparticles

Thermophysical Properties	Blood	Gold	Copper
Density $[\rho(kg/m^3)]$	1063	19320	8933
Thermal Conductivity [K(W/mK)]	0.492	314	400
Electrical Conductivity $[\sigma(S/m)]$	0.667	4.10×10^7	5.96×10^7
Thermal Expansion Coefficient $[\gamma \times 10^{-5}(K^{-1})]$	0.18	1.4	1.67
Heat Capacitance $[C_p(J/kgK)]$	3594	129	385

2.2 Non-dimensionalization

The governing equations given by (6)–(9) need to be transformed into dimensionless form so that a numerical solution for these equations can be obtained. The following dimensionless variables are introduced:

$$\bar{r}_1^* = \frac{r_1^*}{R_0}, \bar{w}_1^* = \frac{w_1^*}{U_0}, \bar{u}_1^* = \frac{L_0 u_1^*}{\delta^* U_0}, \bar{t}_1^* = \frac{U_0 t_1^*}{R_0}, \bar{z}_1^* = \frac{z_1^*}{L_0}, \bar{p}_1^* = \frac{R_0^2 p_1^*}{U_0 L_0 \mu_f}, \tilde{\theta} = \frac{\tilde{T}^* - \tilde{T}_1^*}{\tilde{T}_w^* - \tilde{T}_1^*},$$
$$\bar{R} = \frac{R}{R_0}, \alpha = \frac{\alpha^* L_0}{R_0}, \bar{d} = \frac{d}{L_0}, \bar{w}_s = \frac{w_s}{U_0}, Re = \frac{U_0 \rho_f R_0}{\mu_f}, M^2 = \frac{\sigma_f B_0^2 R_0^2}{\mu_f},$$
$$Gr = \frac{\rho_f R_0^2 g \gamma_f (\tilde{T}_w^* - \tilde{T}_1^*)}{\mu_f U_0}, Pr = \frac{\mu_f C_p}{k_f}, Nr = \frac{16\sigma_e \tilde{T}_1^{*3}}{3k_f k_e}. \tag{14}$$

The insertion of the above non-dimensional parameters mentioned in (14), disregarding the bars and using the mild stenotic hypotheses that the maximal stenosis height is less than the artery's radius, i.e., $\delta(= \delta^*/R_0) << 1$, and the artery's radius and the stenotic region's length are proportionate, i.e., $\epsilon(=$

$R_0/L_0) = O(1)$ leads to the modified form of governing Eqs. (6)–(9), which are as follows:

Continuity Equation:

$$\frac{\partial w_1^*}{\partial z_1^*} = 0, \tag{15}$$

Momentum Equation:
r-direction:

$$\frac{\partial p_1^*}{\partial r_1^*} = 0, \tag{16}$$

z-direction:

$$Re\frac{\rho_{hnf}}{\rho_f}\frac{\partial w_1^*}{\partial t_1^*} = -\frac{\partial p_1^*}{\partial z_1^*} + \frac{1}{2r_1^*}\frac{\partial}{\partial r_1^*}\left[\frac{\mu_{hnf}}{\mu_f}\left(1+\frac{1}{\beta}\right)r_1^*\frac{\partial w_1^*}{\partial r_1^*}\right] + \frac{(\rho\gamma)_{hnf}}{(\rho\gamma)_f}Gr\tilde{\theta} - \frac{\sigma_{hnf}}{\sigma_f}M^2 w_1^*, \tag{17}$$

Energy Equation:

$$\frac{(\rho C_p)_{hnf}}{(\rho C_p)_f}\frac{\partial\tilde{\theta}}{\partial t_1^*} = \frac{1}{RePr}\frac{k_{hnf}}{k_f}\left[\frac{\partial^2\tilde{\theta}}{\partial r_1^{*2}} + \frac{1}{r_1^*}\frac{\partial\tilde{\theta}}{\partial r_1^*}\right] + \frac{Nr}{RePr}\frac{\partial^2\tilde{\theta}}{\partial r_1^{*2}}. \tag{18}$$

The geometry of stenosis in the dimensionless form can be described as:

$$R(z_1^*) = \begin{cases} 1 - \frac{64}{10}\eta_1\left(\frac{11}{32}(z_1^*-d) + \frac{47}{48}(z_1^*-d)^2 - (z_1^*-d)^3 + \frac{1}{3}(z_1^*-d)^4\right), \\ \qquad\qquad\qquad\qquad\qquad\qquad d \le z_1^* \le d + 3/2, \\ 1, \qquad\qquad\qquad\qquad\qquad\qquad \text{otherwise.} \end{cases} \tag{19}$$

where

$$\eta_1 = 4\delta, \quad \delta = \frac{\delta^*}{R_0}.$$

Blood flows through the cardiovascular system due to the heart's pumping motion, causing a pressure gradient across the vascular network. The pressure gradient is separated into two parts: non-fluctuating (continuous) and fluctuating (pulsatile) [28] as given below:

$$-\frac{\partial p_1^*}{\partial z_1^*} = A_0 + A_1 cos(w_p t_1^*), t_1^* > 0, \tag{20}$$

where, A_0 and A_1 signify the amplitudes of the steady-state and pulsatile pressure gradient components, respectively, and $w_p = 2\pi f_p$, f_p depicts the heart pulse frequency.

On the substitution of dimensionless variables given in (14), the modified equation for the pressure gradient becomes:

$$-\frac{\partial p_1^*}{\partial z_1^*} = B_1[1 + ecos(c_1 t_1^*)], \tag{21}$$

where

$$e = \frac{A_1}{A_0}, B_1 = \frac{A_0 R_0^2}{\mu_0 U_0}, c_1 = \frac{2\pi R_0 f_p}{U_0}. \tag{22}$$

Using Eq. (21) in Eq. (17), we have:

$$Re\frac{\rho_{hnf}}{\rho_f}\frac{\partial w_1^*}{\partial t_1^*} = B_1[1 + ecos(c_1 t_1^*)] - \frac{1}{2}\left(1 + \frac{1}{\beta}\right)\frac{m\beta_1 h_m (r_1^*)^{m-1}}{(1-\phi_1)^{2.5}(1-\phi_2)^{2.5}}\frac{\partial w_1^*}{\partial r_1^*} + \frac{1}{2}\frac{\mu_{hnf}}{\mu_f}\left(1 + \frac{1}{\beta}\right)\frac{1}{r_1^*}\frac{\partial}{\partial r_1^*}\left(r_1^*\frac{\partial w_1^*}{\partial r_1^*}\right) + \frac{(\rho\gamma)_{hnf}}{(\rho\gamma)_f}Gr\tilde{\theta} - \frac{\sigma_{hnf}}{\sigma_f}M^2 w_1^*. \tag{23}$$

2.3 Radial Coordinate Transformation

The physical geometry taken into account in the formulated problem is cylindrical, i.e., a cylindrical coordinate system is considered. However, in order to use the computational approach, the considered geometry needs to be transformed into a rectangular domain by employing the transformation $\left(x_1^* = \frac{r_1^*}{R(z_1^*)}\right)$. On applying this transformation, the Eqs. (23) and (18) become:

$$Re\frac{\rho_{hnf}}{\rho_f}\frac{\partial w_1^*}{\partial t_1^*} = B_1[1 + ecos(c_1 t_1^*)] - \frac{1}{2}\left(1 + \frac{1}{\beta}\right)\frac{m\beta_1 h_m R^{m-2}(x_1^*)^{m-1}}{(1-\phi_1)^{2.5}(1-\phi_2)^{2.5}}\frac{\partial w_1^*}{\partial x_1^*} + \frac{1}{2}\frac{1+\beta_1 h_m[1 - R^m(x_1^*)^m]}{(1-\phi_1)^{2.5}(1-\phi_2)^{2.5}}\left(1 + \frac{1}{\beta}\right)\left(\frac{1}{R^2}\right)\left[\frac{\partial^2 \tilde{w_1^*}}{\partial x_1^{*2}} + \frac{1}{x_1^*}\frac{\partial \tilde{w_1^*}}{\partial x_1^*}\right] + \frac{(\rho\gamma)_{hnf}}{(\rho\gamma)_f}Gr\tilde{\theta} - \frac{\sigma_{hnf}}{\sigma_f}M^2 w_1^*, \tag{24}$$

$$\frac{(\rho C_p)_{hnf}}{(\rho C_p)_f}\frac{\partial \tilde{\theta}}{\partial t_1^*} = \frac{1}{RePr}\frac{k_{hnf}}{k_f}\left(\frac{1}{R^2}\right)\left[\frac{\partial^2 \tilde{\theta}}{\partial x_1^{*2}} + \frac{1}{x_1^*}\frac{\partial \tilde{\theta}}{\partial x_1^*}\right] + \left(\frac{1}{R^2}\right)\frac{Nr}{RePr}\frac{\partial^2 \tilde{\theta}}{\partial x_1^{*2}}. \tag{25}$$

The boundary conditions mentioned in Eq. (11) and (12) are reduced as follows:

$$\left.\frac{\partial w_1^*}{\partial x_1^*}\right|_{x_1^*=0} = 0,\ w_1^*|_{x_1^*=-1,1} = w_s,\ \left.\frac{\partial \tilde{\theta}}{\partial x_1^*}\right|_{x_1^*=0} = 0,\ \tilde{\theta}|_{x_1^*=-1,1} = 1. \tag{26}$$

The wall shear stress (WSS) and volumetric flow rate are expressed as:

$$\tau_w = -\frac{1}{R}\left(1 + \frac{1}{\beta}\right)\left(\frac{\partial w_1^*}{\partial x_1^*}\right)_{x_1^*=1} \tag{27}$$

$$Q_1 = 2\pi R^2 \int_0^1 w_1^* x_1^* dx_1^*, \tag{28}$$

3 Solution Process

The partial differential Eqs. (24) and (25) are coupled differential equations; therefore, obtaining an analytic solution is too difficult. On the other hand, numerical approaches can yield a highly accurate solution. An unconditionally stable implicit finite difference (Crank-Nicolson) approach is used in this case. The subscripts and superscripts in Eqs. (24) and (25) are ignored for discretization.

3.1 Discretization

On employing the values of thermophysical parameters of hybrid nanofluid from Table 1 and discretizing the governing Eqs. (24) and (25) using the Crank-Nicolson scheme, the desired form of equations is:

$$\begin{aligned}
&\left[(1-\phi_2)\left[(1-\phi_1)+\phi_1\frac{\rho_{s1}}{\rho_f}\right]+\phi_2\frac{\rho_{s2}}{\rho_f}\right]Re\left[\frac{w_i^{k+1}-w_i^k}{dt}\right]=B_1[1+ecos(c_1t^k)]\\
&-\frac{1}{2}\left(1+\frac{1}{\beta}\right)\frac{m\beta_1h_mR^{m-2}(x(i))^{m-1}}{(1-\phi_1)^{2.5}(1-\phi_2)^{2.5}}\left[\frac{1}{2}\left(\frac{w_{i+1}^{k+1}-w_{i-1}^{k+1}}{2dx}+\frac{w_{i+1}^{k}-w_{i-1}^{k}}{2dx}\right)\right]\\
&+\frac{1}{2}\left(1+\frac{1}{\beta}\right)\frac{1+\beta_1h_m[1-R^m(x(i))^m]}{(1-\phi_1)^{2.5}(1-\phi_2)^{2.5}}\left(\frac{1}{R^2}\right)\left[\frac{1}{2}\left(\frac{w_{i+1}^{k+1}-2w_i^{k+1}+w_{i-1}^{k+1}}{dx^2}\right.\right.\\
&\left.\left.+\frac{w_{i+1}^{k}-2w_i^{k}+w_{i-1}^{k}}{dx^2}\right)+\frac{1}{2x(i)}\left(\frac{w_{i+1}^{k+1}-w_{i-1}^{k+1}}{2dx}+\frac{w_{i+1}^{k}-w_{i-1}^{k}}{2dx}\right)\right]\\
&+\left[(1-\phi_2)\left[(1-\phi_1)+\phi_1\frac{(\rho\gamma)_{s1}}{(\rho\gamma)_f}\right]+\phi_2\frac{(\rho\gamma)_{s2}}{(\rho\gamma)_f}\right]Gr\tilde{\theta}_i^k-\frac{1}{2}\frac{\sigma_{hnf}}{\sigma_f}M^2(w_i^k+w_i^{k+1}),
\end{aligned}\tag{29}$$

$$\begin{aligned}
&\left[(1-\phi_2)\left[(1-\phi_1)+\phi_1\frac{(\rho C_p)_{s1}}{(\rho C_p)_f}\right]+\phi_2\frac{(\rho C_p)_{s2}}{(\rho C_p)_f}\right]\left[\frac{\tilde{\theta}_i^{k+1}-\tilde{\theta}_i^k}{dt}\right]\\
&=\frac{1}{RePr}\left(\frac{k_{hnf}}{k_f}+Nr\right)\left(\frac{1}{R^2}\right)\left[\frac{1}{2}\left(\frac{\tilde{\theta}_{i+1}^{k+1}-2\tilde{\theta}_i^{k+1}+\tilde{\theta}_{i-1}^{k+1}}{dx^2}+\frac{\tilde{\theta}_{i+1}^{k}-2\tilde{\theta}_i^{k}+\tilde{\theta}_{i-1}^{k}}{dx^2}\right)\right.\\
&\left.+\frac{1}{2x(i)}\left(\frac{\tilde{\theta}_{i+1}^{k+1}-\tilde{\theta}_{i-1}^{k+1}}{2dx}+\frac{\tilde{\theta}_{i+1}^{k}-\tilde{\theta}_{i-1}^{k}}{2dx}\right)\right].
\end{aligned}\tag{30}$$

The Crank-Nicolson scheme employed in the current analysis is, however, stable for all values for dt and dx still, a minimal value is considered with great precision as $dt = 10^{-4}$ and $dx = 10^{-4}$. It is noticed that no further change occurs in the values of hemodynamical parameters studied in the research with decreasing values of dt and dx. A total of $N+1$ grid points have been considered in the spatial direction, with $x = 1/N + 1$ being the step size, whereas $M + 1$

grid points are considered temporal. The value at any time instant t^k is given as $t^k = (k-1)dt$, dt being a small increment in time. As the scheme employed is an implicit one; therefore a system of equations is obtained, and it is in the form of a tri-diagonal system which can be solved with the Tri-diagonal Matrix Algorithm (TDMA) [29].

The tri-diagonal system corresponding to Eq. (29) is given by

$$A_i^k w_{i-1}^{k+1} + B_i^k w_i^{k+1} + C_i^k w_{i+1}^{k+1} = A_i^{'k} w_{i-1}^k + B_i^{'k} w_i^k + C_i^{'k} w_{i+1}^k + D_i^k, \qquad (31)$$

where

$A_i^k = -\frac{1+\beta_1 h_m[1-R^m(x(i))^m]}{(1-\phi_1)^{2.5}(1-\phi_2)^{2.5}}\left(\frac{1}{4R^2}\right)\left(\frac{dt}{dx^2} - \frac{1}{2x(i)}\frac{dt}{dx}\right) - \frac{dt}{8dx}\left(1+\frac{1}{\beta}\right)\frac{m\beta_1 h_m R^{m-2}(x(i))^{m-1}}{(1-\phi_1)^{2.5}(1-\phi_2)^{2.5}},$

$B_i^k = Re\left[(1-\phi_2)\left[(1-\phi_1)+\phi_1\frac{\rho_{s1}}{\rho_f}\right]+\phi_2\frac{\rho_{s2}}{\rho_f}\right] + \frac{1+\beta_1 h_m[1-R^m(x(i))^m]}{(1-\phi_1)^{2.5}(1-\phi_2)^{2.5}}\frac{1}{2R^2}\frac{dt}{dx^2} + \frac{dt}{2}\frac{\sigma_{hnf}}{\sigma_f}M^2,$

$C_i^k = -\frac{1+\beta_1 h_m[1-R^m(x(i))^m]}{(1-\phi_1)^{2.5}(1-\phi_2)^{2.5}}\left(\frac{1}{4R^2}\right)\left(\frac{dt}{dx^2} + \frac{1}{2x(i)}\frac{dt}{dx}\right) + \frac{dt}{8dx}\left(1+\frac{1}{\beta}\right)\frac{m\beta_1 h_m R^{m-2}(x(i))^{m-1}}{(1-\phi_1)^{2.5}(1-\phi_2)^{2.5}},$

$A_i^{'k} = \frac{1+\beta_1 h_m[1-R^m(x(i))^m]}{(1-\phi_1)^{2.5}(1-\phi_2)^{2.5}}\left(\frac{1}{4R^2}\right)\left(\frac{dt}{dx^2} - \frac{1}{2x(i)}\frac{dt}{dx}\right) + \frac{dt}{8dx}\left(1+\frac{1}{\beta}\right)\frac{m\beta_1 h_m R^{m-2}(x(i))^{m-1}}{(1-\phi_1)^{2.5}(1-\phi_2)^{2.5}},$

$B_i^{'k} = Re\left[(1-\phi_2)\left[(1-\phi_1)+\phi_1\frac{\rho_{s1}}{\rho_f}\right]+\phi_2\frac{\rho_{s2}}{\rho_f}\right] - \frac{1+\beta_1 h_m[1-R^m(x(i))^m]}{(1-\phi_1)^{2.5}(1-\phi_2)^{2.5}}\frac{1}{2R^2}\frac{dt}{dx^2} - \frac{dt}{2}\frac{\sigma_{hnf}}{\sigma_f}M^2,$

$C_i^{'k} = \frac{1+\beta_1 h_m[1-R^m(x(i))^m]}{(1-\phi_1)^{2.5}(1-\phi_2)^{2.5}}\left(\frac{1}{4R^2}\right)\left(\frac{dt}{dx^2} + \frac{1}{2x(i)}\frac{dt}{dx}\right) - \frac{dt}{8dx}\left(1+\frac{1}{\beta}\right)\frac{m\beta_1 h_m R^{m-2}(x(i))^{m-1}}{(1-\phi_1)^{2.5}(1-\phi_2)^{2.5}},$

$D_i^k = dtB_1[1+ecos(c_1 t^k)] + dt\left[(1-\phi_2)\left[(1-\phi_1)+\phi_1\frac{(\rho\gamma)_{s1}}{(\rho\gamma)_f}\right]+\phi_2\frac{(\rho\gamma)_{s2}}{(\rho\gamma)_f}\right]Gr\tilde{\theta}_i^k.$

The tri-diagonal system corresponding to Eq. (30) is given by

$$P_i^k \theta_{i-1}^{k+1} + Q_i^k \theta_i^{k+1} + S_i^k \theta_{i+1}^{k+1} = P_i^{'k} \theta_{i-1}^k + Q_i^{'k} \theta_i^k + S_i^{'k} \theta_{i+1}^k + F_i^k, \qquad (32)$$

where

$P_i^k = -\frac{1}{RePr}\left(\frac{1}{2R^2}\right)\left(\frac{k_{hnf}}{k_f}+Nr\right)\left(\frac{dt}{dx^2} - \frac{1}{2x(i)}\frac{dt}{dx}\right),$

$Q_i^k = \left[(1-\phi_2)\left[(1-\phi_1)+\phi_1\frac{(\rho C_p)_{s1}}{(\rho C_p)_f}\right]+\phi_2\frac{(\rho C_p)_{s2}}{(\rho C_p)_f}\right] + \frac{1}{RePr}\frac{1}{R^2}\frac{dt}{dx^2}\left(\frac{k_{hnf}}{k_f}+Nr\right),$

$S_i^k = -\frac{1}{RePr}\left(\frac{1}{2R^2}\right)\left(\frac{k_{hnf}}{k_f}+Nr\right)\left(\frac{dt}{dx^2} + \frac{1}{2x(i)}\frac{dt}{dx}\right),$

$P_i^{'k} = \frac{1}{RePr}\left(\frac{1}{2R^2}\right)\left(\frac{k_{hnf}}{k_f}+Nr\right)\left(\frac{dt}{dx^2} - \frac{1}{2x(i)}\frac{dt}{dx}\right),$

$Q_i^{'k} = \left[(1-\phi_2)\left[(1-\phi_1)+\phi_1\frac{(\rho C_p)_{s1}}{(\rho C_p)_f}\right]+\phi_2\frac{(\rho C_p)_{s2}}{(\rho C_p)_f}\right] - \frac{1}{RePr}\frac{1}{R^2}\frac{dt}{dx^2}\left(\frac{k_{hnf}}{k_f}+Nr\right),$

$S_i^{'k} = \frac{1}{RePr}\left(\frac{1}{2R^2}\right)\left(\frac{k_{hnf}}{k_f}+Nr\right)\left(\frac{dt}{dx^2} + \frac{1}{2x(i)}\frac{dt}{dx}\right),$

$F_i^k = 0.$

4 Results and Graphical Analysis

The effect of various flow-related parametric parameters, including the hematocrit parameter (h_m), wall slip velocity (w_s), Casson fluid parameter (β), volume fractions of both nanoparticles (ϕ_1, ϕ_2), radiation parameter (Nr), and Prandtl number (Pr), on non-dimensional velocity, non-dimensional temperature, wall shear stress, and flow rate, are covered in this section. Au-Blood, a unitary nanofluid, and Au-Cu/Blood, a hybrid nanofluid, have been compared. The values of the emergent parameters employed in the analysis are shown in Table 2. Table 3 lists the values for the thermophysical characteristics of the blood, Au, and Cu nanoparticles.

To validate the study conducted, the numerical scheme (Crank-Nicolson) used must be verified. In the absence of a few physical parameters, the current model reduces the ones published in the literature. As the Casson fluid parameter in the current work approaches infinity ($\beta \to \infty$), the current model approaches the Newtonian model in [27]. The hematocrit parameter (h_m) in the present analysis and viscosity parameter (β_0) in [27] have been neglected to verify the results. The numerical scheme has also been validated for Au-nanoparticles used in both research works. The effect of inclination of the magnetic field, Joule heating, and viscous dissipation in [27] has been ignored. Figure 2a & 2b have been plotted for verification. The findings of comparison with existing literature results [27] indicate good agreement, which supports the validity of the current solutions.

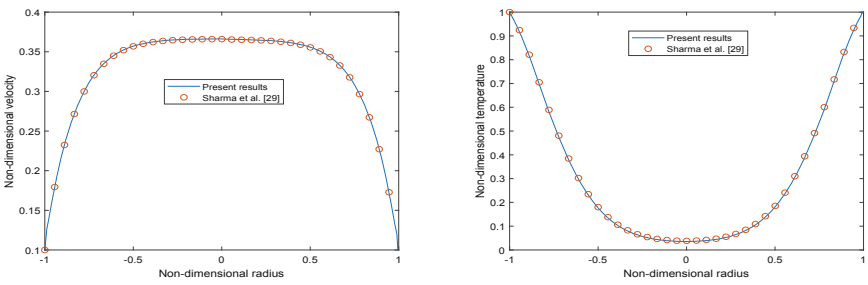

(a) (b)

Fig. 2. Comparative study (a) velocity profile ($M^2 = 1$), (b) temperature profile (Ec = 0.2).

The effect of various flow parameters such as hematocrit parameter (h_m), wall slip velocity (w_s), Casson fluid parameter (β), and volume fractions of both the nanoparticles (ϕ_1, ϕ_2) on non-dimensional velocity profiles is portrayed in Fig. 3. A comparative analysis has been performed between unitary nanofluid (Au-Blood) and hybrid nanofluid (Au-Cu/Blood). Blood velocity distribution

for various h_m values is shown in a radial direction in Fig. 3a. Blood viscosity is significantly influenced by the hematocrit measure (h_m). Both the hematocrit-dependent ($h_m \neq 0$) and constant ($h_m = 0$) scenarios have been studied. The hybrid blood velocity is larger when $h_m = 0$ and falls as h_m increases, according to Fig. 3a. With an increase in h_m levels, the viscosity of the blood increases, which impedes blood flow; a drop in velocity profiles is examined with h_m. Additionally, greater magnitudes of the hybrid nanofluid (Au-Cu/Blood) have been observed than those of the unitary nanofluid (Au-Blood). The velocity is at its peak near the artery's centerline, gradually decreasing until it approaches the vessel wall, reaching the wall slip velocity (w_s). Figure 3b depicts the effect of w_s on non-dimensional velocity profiles. With an increase in the slip parameter w_s, the axial flow accelerates significantly as the hydrodynamic wall slip effect increases. No-slip velocity is typically considered at the artery wall, which has the least significance. As a result, the wall slip has been introduced at the arterial wall in the current investigation using boundary conditions. The artery's core region exhibits the highest flow velocity, which decreases as it gets closer to the arterial wall. Figure 3c shows how β affects the non-dimensional velocity profile. The velocity field rises as the β expands since the velocity field's boundary layer thickness decreases. It is so because HNF becomes more viscous, and its elasticity increases as the value of β rise. Figure 3d displays the non-dimensional velocity profiles for various values of ϕ_1, ϕ_2. The volume fraction of both Au- and Cu-nanoparticles rises along with the velocity profiles. When $\phi_1 = 0.01, \phi_2 = 0.01$, the velocity value is the lowest, and when $\phi_1 = 0.05, \phi_2 = 0.05$, the velocity value is the highest.

Figure 4 illustrates the impact of several flow parameters, including the radiation parameter (Nr), Prandtl number (Pr), Casson fluid parameter (β), and volume fractions of both the nanoparticles (ϕ_1, ϕ_2) on non-dimensional temperature profiles. The effect of Nr on non-dimensional temperature profiles is depicted in Fig. 4a. With rising values of Nr, there is an increase in temperature profiles. Additionally, Au-Cu/Blood hybrid nanofluid reaches higher magnitudes than Au-Blood nanofluid. The system emits the most heat due to the inverse effect of Nr on thermal conductivity. Radiation serves as a heat source within the bloodstream. Hence an increase in radiation exposure elevates body temperature. When light with the proper wavelength interacts with nanoparticles, the free electrons within the nanoparticles vibrate. These oscillations generate heat that kills malignant cells by spreading over the surrounding environment. This discovery has extensive thermal therapeutic applications. Figure 4b highlights how Pr affects the non-dimensional temperature profile. An increase in Pr values accompanies the declination of the temperature profiles since the thermal boundary layer thickness decreases with Pr. The viscosity and thermal diffusivity of the fluid determine Pr. The momentum transport is linked to heat transport through this dimensionless quantity. The Prandtl number tells us how heat diffuses faster, i.e., whether heat conduction or convection is more prominent in a fluid. The physical importance of the Prandtl number is that when it is smaller than 1, conductive heat transfer becomes the more prominent process,

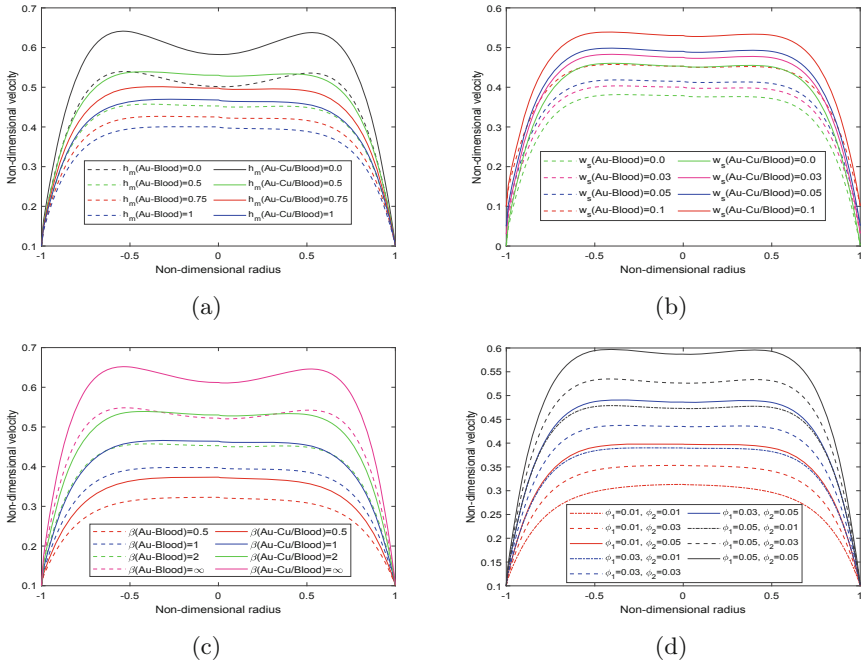

Fig. 3. Effect of (a) hematocrit parameter (h_m), (b) wall slip velocity (w_s), (c) Casson fluid parameter (β), (d) volume fractions of both nanoparticles (ϕ_1, ϕ_2) on non-dimensional velocity at $z_1^* = 1.31$ and $t_1^* = 1.2$

i.e., conduction transfers a higher proportion of heat than convection. Convective heat transfer is more significant than conduction when the Prandtl value is greater than 1. The effect of β on the temperature profile is illustrated in Fig. 4c. The fluid's temperature increases with an increase in β because the thickness of the thermal boundary layer increases with an increment in values of β. Figure 4d shows the impact of ϕ_1, ϕ_2 on non-dimensional temperature profiles. When the volume percentage of both nanoparticles increases, the temperature profiles also show enhancement. The temperature demonstrates minimal value for $\phi_1 = 0.01, \phi_2 = 0.01$, and a maximum value for $\phi_1 = 0.05, \phi_2 = 0.05$, highlighting the importance of both nanoparticles in regulating the temperature.

The time series plots for wall shear stress (WSS) and volumetric flow rate at the stenosis region are shown in Fig. 5. These graphs depict the oscillating character of blood flow in the stenotic zone as time passes. The graphs demonstrate that the magnitude initially declines before exhibiting an ascending trend sustained throughout time after a crucial point in time. The influence of w_s on WSS and flow rate is represented in Fig. 5a and 5b. Figure 5a depicts that WSS decreases dramatically with increment in w_s values, with minor backflow. As a result, as w_s rises, the beginning value of WSS profiles lowers by a certain amount. Figure 5b illustrates that raising the wall slip parameter causes a

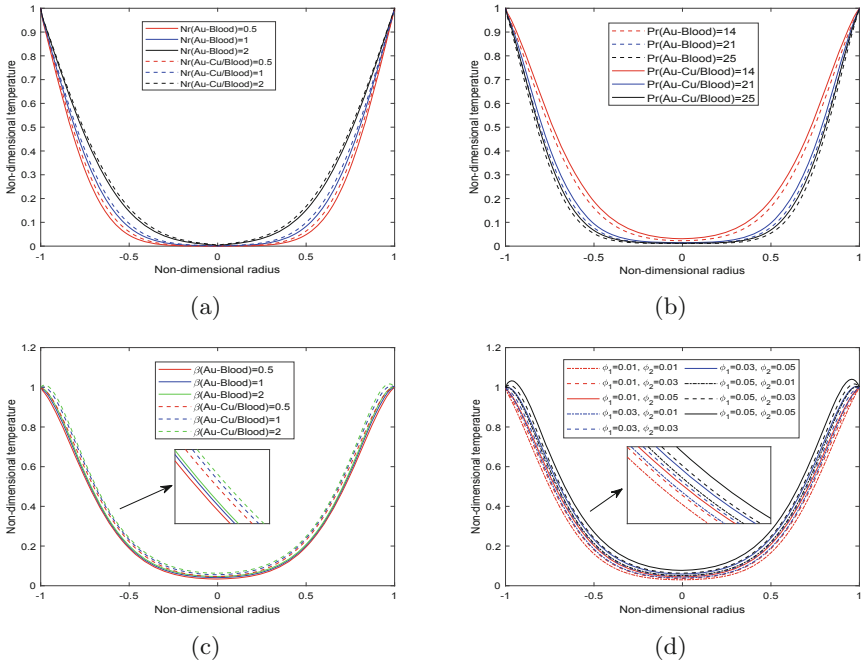

Fig. 4. Effect of (a) Radiation parameter (Nr), (b) Prandtl number (Pr), (c) Casson fluid parameter (β), (d) different concentrations of both nanoparticles (ϕ_1, ϕ_2) on temperature profiles at $z_1^* = 1.31$ and $t_1^* = 1.2$

significantly more pronounced increase in volumetric flow rate, implying that significant growth in flux is driven by increasing wall slip. The impact of the volume fraction of Au-nanoparticles (ϕ_1) on WSS and volumetric flow rate is depicted in Fig. 5c and 5d. It is analyzed that there is a decrement in WSS and flow rate initially up to a certain point of time with increasing values of ϕ_1, but then it rises over time. Figures 5e and 5f highlight the variations of WSS and flow rate profiles for various hybrid nanoparticle combinations. The patterns show that when the nanoparticles' volume fraction rises simultaneously, the oscillatory wall shear stress profiles reduce in magnitude up to a certain threshold, increasing with time. The profiles for flow rate exhibit the same trend as that of WSS, as presented in Fig. 5f.

The influence of the hematocrit parameter (h_m) and stenotic depth (δ) on wall shear stress and flow rate concerning arterial length is highlighted in Fig. 6. The WSS profiles for h_m are depicted in Fig. 6a. A declination in WSS values is analyzed with increasing h_m values since the fluid's viscosity is enhanced. Moreover, Fig. 6b manifests that the flow rate profiles also decline with an increment in h_m values since the increased viscosity hinders the flow of the fluid (blood). Figure 6c depicts the influence of δ on WSS profiles. According to Zhang et al. [30], the WSS reduces as δ increases, indicating that lower shear stress levels are

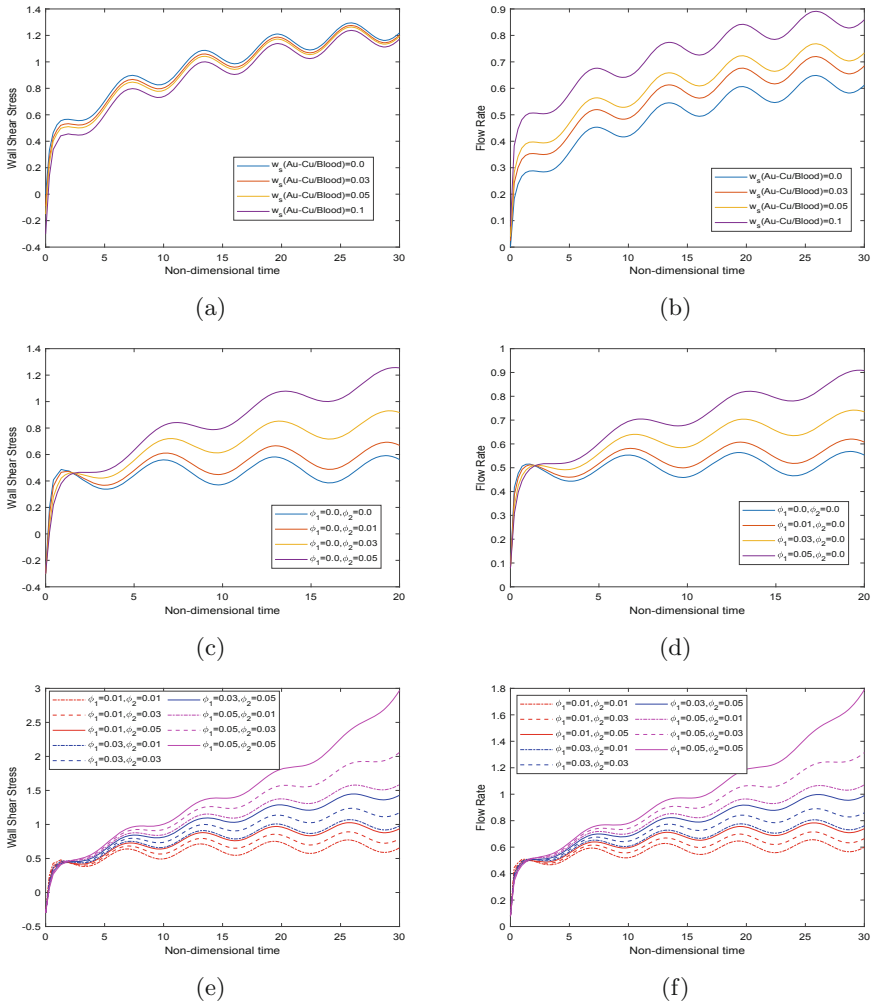

Fig. 5. Effect of (a, b) wall slip velocity (w_s), (c, d) volume fraction of Au-nanoparticles (ϕ_1) (e,f) volume fraction of both nanoparticles (ϕ_1, ϕ_2) on wall shear stress and flow rate with respect to time

more harmful. The effect of δ on flow rate profiles is presented in Fig. 6d. It is seen that flow rate profiles decline with an increase in δ values.

This section aims to analyze how the blood flows in the stenotic zone and how it behaves in other parts of the artery. Also, hybrid nanoparticles are inserted to boost drug delivery and treat atherosclerosis. The impact of flow parameters such as hematocrit parameter (h_m), Casson fluid parameter (β), and volume fraction of both the nanoparticles (ϕ_1,ϕ_2) is illustrated via velocity contours in Fig. 7, 8, 9. The effect of h_m is highlighted in Fig. 7. Figure 7a depicts the constant viscosity case (h_m=0), and the maximum velocity value is observed in this case.

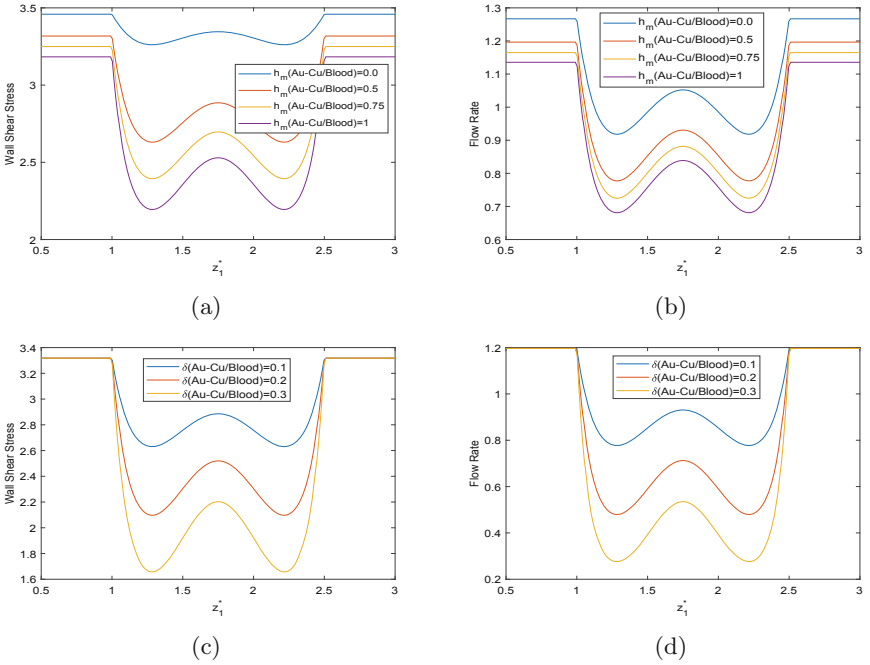

Fig. 6. Effect of Effect of (a, b) hematocrit parameter (h_m), and (c, d) stenotic depth (δ) on wall shear stress and flow rate at $t_1^* = 1.2$

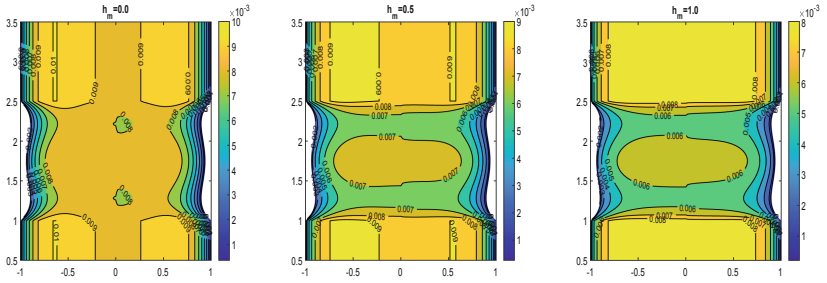

Fig. 7. Velocity contours for (a) $h_m = 0.0$, (b) $h_m = 0.5$, (c) $h_m = 1.0$

The velocity profiles decline with increasing h_m values since viscosity enhances and flow retardation occurs. The velocity contours for β are represented by Fig. 8. As β increases, the boundary layer thickness of the velocity field decreases, increasing velocity. Figure 9 highlights the velocity contours for different combinations of ϕ_1 and ϕ_2. It is analyzed that the velocity increases with an increase in the volume fraction of both nanoparticles. Figure 9a shows the contour for the pure-blood case, i.e., when no nanoparticle is injected into the bloodstream. The

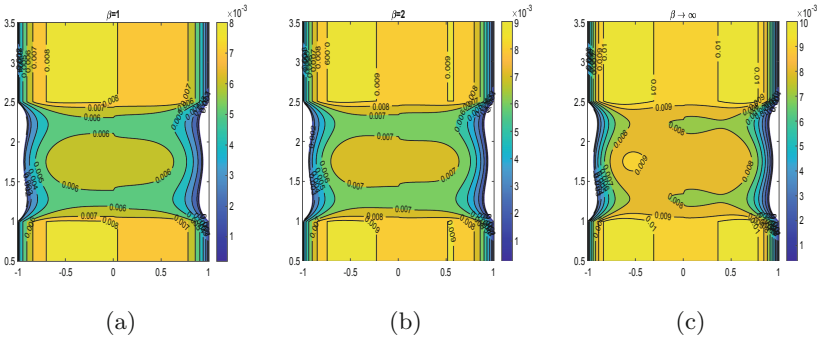

Fig. 8. Velocity contours for (a) $\beta = 1$, (b) $\beta = 2$, (c) $\beta \to \infty$

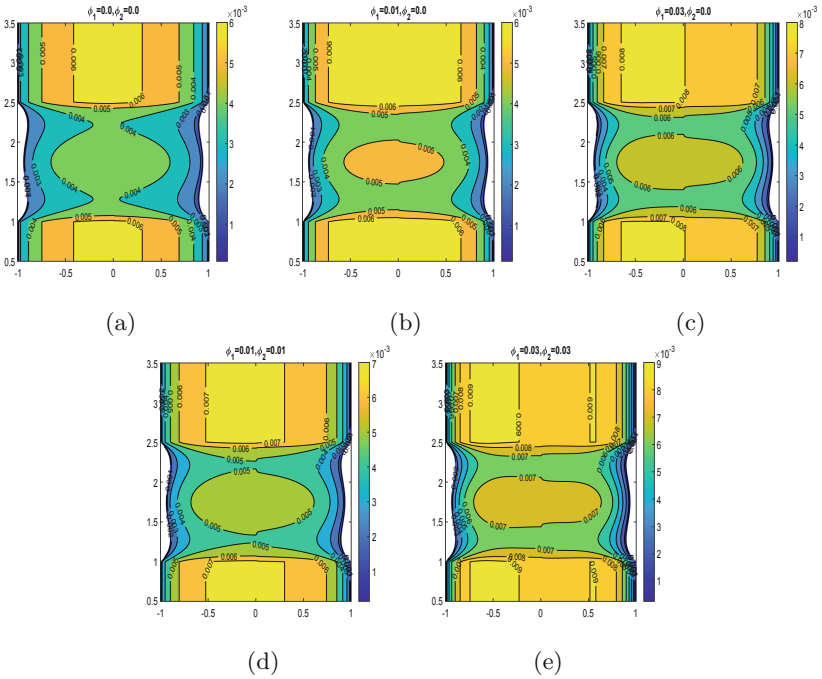

Fig. 9. Velocity contours for (a) $\phi_1 = 0.0$, $\phi_2 = 0.0$, (b) $\phi_1 = 0.01$, $\phi_2 = 0.0$, (c) $\phi_1 = 0.03$, $\phi_2 = 0.0$, (d) $\phi_1 = 0.01$, $\phi_2 = 0.01$, (e) $\phi_1 = 0.03$, $\phi_2 = 0.03$

formation of the trapped bolus is visible in the stenotic zone when comparing the pure-blood and nanoparticle cases. Also, the trapped bolus's size increases with an increase in the volume fraction of both nanoparticles.

5 Conclusions

In this study, hybrid nanoparticles (Au+Cu) of various shapes are used to evaluate the impacts of wall slip effects on blood flow through an overlapping stenosed artery. It is assumed that the blood viscosity varies with hematocrit. Additionally, as blood is thought to be non-Newtonian, it is modeled using the Casson fluid model, which accurately captures the properties of real blood. The Crank-Nicolson approach is used to discretize the governing equations before MATLAB is used to solve them. Graphical representations of the results, including contour plots, are used. According to the findings mentioned above, the following observations are made:

- The Au-Cu/Blood hybrid nanofluid reaches constantly higher magnitudes than Au-Blood nanofluid for the velocity and temperature profiles.
- The velocity profile show declination with h_m whereas the opposite trend is noticed for β.
- The WSS profiles elevate with w_s while the reverse trend is analyzed for flow rate profiles.
- WSS and flow rate profiles show elevation with ϕ_1.
- The temperature profiles show enhancement with β and Nr.
- There is an increment in velocity and temperature profile with increase in ϕ_1 and ϕ_2 simultaneously.

Future Work. The current study may be extended to include a permeable bifurcated artery with stenosis in the parent and daughter artery while considering the shape and size of the nanoparticles influenced by external factors such as an applied electric field, Joule heating, heat source, and viscous dissipation.

References

1. Ghosh, P., Han, G., De, M., Kim, C.K., Rotello, V.M.: Gold nanoparticles in delivery applications. Adv. Drug Deliv. Rev. **60**(11), 1307–1315 (2008)
2. Gentile, F., Ferrari, M., Decuzzi, P.: The transport of nanoparticles in blood vessels: the effect of vessel permeability and blood rheology. Ann. Biomed. Eng. **36**(2), 254–261 (2008). https://doi.org/10.1007/s10439-007-9423-6
3. Ijaz, S., Nadeem, S.: Slip examination on the wall of tapered stenosed artery with emerging application of nanoparticles. Int. J. Therm. Sci. **109**, 401–412 (2016)
4. Bahrami, B., et al.: Nanoparticles and targeted drug delivery in cancer therapy. Immunol. Lett. **190**, 64–83 (2017)
5. Gupta, S., Kumar, D., Singh, J.: Analytical study for MHD flow of Williamson nanofluid with the effects of variable thickness, nonlinear thermal radiation and improved Fourier's and Fick's laws. SN Appl. Sci. **2**(3), 1–12 (2020). https://doi.org/10.1007/s42452-020-1995-x
6. Umadevi, C., Dhange, M., Haritha, B., Sudha, T.: Flow of blood mixed with copper nanoparticles in an inclined overlapping stenosed artery with magnetic field. Case Stud. Thermal Eng. **25**, 100947 (2021)

7. Ghandi, R., Sharma, B.K., Kumawat, C., Beg, O.A.: Modeling and analysis of magnetic hybrid nanoparticle (Au–Al_2O_3/blood) based drug delivery through a bell-shaped occluded artery with Joule heating, viscous dissipation and variable viscosity effects. Proc. Inst. Mech. Eng., Part E: J. Process Mech. Eng. 09544089221080273 (2022)
8. Gandhi, R., Sharma, B.K.: Unsteady MHD hybrid nanoparticle (Au–Al_2O_3/blood) mediated blood flow through a vertical irregular stenosed artery: Drug delivery applications. In: Banerjee, S., Saha, A. (eds.) Nonlinear Dynamics and Applications. Springer Proceedings in Complexity, pp. 325–337. Springer, Cham (2022). https://doi.org/10.1007/978-3-030-99792-2_28
9. Khanduri, U., Sharma, B.K.: Hall and ion slip effects on hybrid nanoparticles (au-go/blood) flow through a catheterized stenosed artery with thrombosis. Proc. Inst. Mech. Eng., Part C: J. Mech. Eng. Sci. 09544062221136710 (2022)
10. Layek, G.C., Mukhopadhyay, S., Gorla, R.S.R.: Unsteady viscous flow with variable viscosity in a vascular tube with an overlapping constriction. Int. J. Eng. Sci. **47**(5–6), 649–659 (2009)
11. Riahi, D.N., Roy, R., Cavazos, S.: On arterial blood flow in the presence of an overlapping stenosis. Math. Comput. Model. **54**(11–12), 2999–3006 (2011)
12. GC Shit and Sreeparna Majee: Pulsatile flow of blood and heat transfer with variable viscosity under magnetic and vibration environment. J. Magn. Magn. Mater. **388**, 106–115 (2015)
13. Zaman, A., Ali, N., Sajid, M.: Numerical simulation of pulsatile flow of blood in a porous-saturated overlapping stenosed artery. Math. Comput. Simul. **134**, 1–16 (2017)
14. Sharma, M., Sharma, B.K., Gaur, R.K., Tripathi, B.: Soret and Dufour effects in biomagnetic fluid of blood flow through a tapered porous stenosed artery. J. Nanofluids **8**(2), 327–336 (2019)
15. Das, S., Pal, T.K., Jana, R.N.: Outlining impact of hybrid composition of nanoparticles suspended in blood flowing in an inclined stenosed artery under magnetic field orientation. BioNanoScience **11**(1), 99–115 (2021). https://doi.org/10.1007/s12668-020-00809-y
16. Zhang, X., Wang, E., Ma, L., Shu, C., Zheng, L.: Analysis of hemodynamics and heat transfer of nanoparticle-injected atherosclerotic patient: considering the drag force and slip between phases of different particle shapes and volume fractions. Int. J. Therm. Sci. **159**, 106637 (2021)
17. Basha, H.T., Rajagopal, K., Ahammad, N.A., Sathish, S., Gunakala, S.R.: Finite difference computation of Au-Cu/magneto-bio-hybrid nanofluid flow in an inclined uneven stenosis artery. Complexity **2022**, 1–18 (2022)
18. Gandhi, R., Sharma, B.K., Makinde, O.D.: Entropy analysis for MHD blood flow of hybrid nanoparticles (Au–Al_2O_3/blood) of different shapes through an irregular stenosed permeable walled artery under periodic body acceleration: Hemodynamical applications. ZAMM-J. Appl. Math. Mecha./Zeitschrift für Angewandte Mathematik und Mechanik e202100532 (2022)
19. Sharma, B.K., Poonam, Chamkha, A.J.: Effects of heat transfer, body acceleration and hybrid nanoparticles (Au–Al_2O_3/blood) on MHD blood flow through a curved artery with stenosis and aneurysm using hematocrit-dependent viscosity. Waves Random Complex Media 1–31 (2022)
20. Chakravarty, S., Mandal, P.K., et al.: Numerical simulation of Casson fluid flow through differently shaped arterial stenoses. Zeitschrift angewandte Math. Phys. **65**(4), 767–782 (2014)

21. Debnath, S., Saha, A.K., Mazumder, B.S., Roy, A.K.: Transport of a reactive solute in a pulsatile non-Newtonian liquid flowing through an annular pipe. J. Eng. Math. **116**(1), 1–22 (2019). https://doi.org/10.1007/s10665-019-09999-1
22. Ali, A., Farooq, H., Abbas, Z., Bukhari, Z., Fatima, A.: Impact of Lorentz force on the pulsatile flow of a non-Newtonian Casson fluid in a constricted channel using Darcy's law: a numerical study. Sci. Rep. **10**(1), 1–15 (2020)
23. Tassaddiq, A., Khan, I., Nisar, K.S., Singh, J.: MHD flow of a generalized Casson fluid with Newtonian heating: a fractional model with Mittag-Leffler memory. Alexandria Eng. J. **59**(5), 3049–3059 (2020)
24. Singh, J., Kumar, D., Baleanu, D., et al.: A hybrid analytical algorithm for thin film flow problem occurring in non-Newtonian fluid mechanics. Ain Shams Eng. J. **12**(2), 2297–2302 (2021)
25. Das, P., Sarifuddin, Rana, J., Mandal, P.K. Solute dispersion in transient Casson fluid flow through stenotic tube with exchange between phases. Phys. Fluids **33**(6), 061907 (2021)
26. Padma, R., Tamil Selvi, R., Ponalagusamy, R.: Electromagnetic control of non-Newtonian fluid (blood) suspended with magnetic nanoparticles in the tapered constricted inclined tube. In: AIP Conference Proceedings, vol. 2336, p. 020008. AIP Publishing LLC (2021)
27. Sharma, B.K., Gandhi, R., Bhatti, M.M.: Entropy analysis of thermally radiating MHD slip flow of hybrid nanoparticles (Au-Al_2O_3/blood) through a tapered multi-stenosed artery. Chem. Phys. Lett. **790**, 139348 (2022)
28. Burton, A.C.: Physiology and biophysics of the circulation. Acad. Med. **40**(8), xxx–xxxvi (1965)
29. Anderson, J.D., Wendt, J.: Computational Fluid Dynamics an Introduction, vol. 206 (1995)
30. Zhang, B., Junyi, G., Qian, M., Niu, L., Zhou, H., Ghista, D.: Correlation between quantitative analysis of wall shear stress and intima-media thickness in atherosclerosis development in carotid arteries. Biomed. Eng. Online **16**(1), 1–17 (2017)